Received: 14 April 2021 | Revised: 22 June 2021 | Accepted: 28 June 2021

DOI: 10.1002/mrm.28929

RESEARCH ARTICLE

Magnetic Resonance in Medicine

NODDI highlights recovery mechanisms in white and gray matter in ischemic stroke following human stem cell treatment

F. Andrew Bagdasarian[1,2] | **Xuegang Yuan**[1,2] | **Jacob Athey**[1,2] | **Bruce A. Bunnell**[3] | **Samuel C. Grant**[1,2]

[1]National High Magnetic Field Laboratory, Florida State University, Tallahassee, Florida, USA

[2]Chemical & Biomedical Engineering, FAMU-FSU College of Engineering, Florida State University, Tallahassee, Florida, USA

[3]Department of Microbiology, Immunology, and Genetics, University of North Texas Health Science Center, Fort Worth, Texas, USA

Correspondence
Samuel C. Grant, National High Magnetic Field Laboratory, Florida State University, 1800 E Paul Dirac Dr, Tallahassee, FL 32310, USA.
Email: grant@magnet.fsu.edu

Funding information
National Institute of Neurological Disorders and Stroke, Grant/Award Number: RO1-NS102395; Division of Materials Research, Grant/Award Number: DMR-1644779

Purpose: Diffusion MRI offers insight into ischemic stroke progression in both human and rodent models. However, diffusion MRI to evaluate therapeutic application of mesenchymal stem cells is limited. Robust analytical techniques are required to identify potential physiological changes as a function of cell therapy in stroke. Here, we seek to establish Neurite Orientation Dispersion and Density Imaging (NODDI) as a feasible method in evaluating stroke evolution in response to cell-based therapeutics.

Methods: Diffusion MRI data at 21.1T were acquired from 16 male rats. Rats were grouped randomly: naïve (baseline, N = 5), stroke with injections of phosphate buffered saline (N = 6), stroke with injection of 2D human mesenchymal stem cells (hMSC, N = 5). Data were acquired on days 1, 3, 7, and 21 post-surgery. DTI and NODDI maps were generated, with regions of interest placed in the ischemic hemisphere external capsule and striatum. Diffusion parameters were compared between groups each day, and within groups across hemispheres and longitudinally. Behavioral characterizations were on days 0 (pre-surgery), 3, 7, 14, and 21.

Results: The 2D hMSC preserved diffusional restriction in the external capsule compared to saline (day 1: MD, $P = .4060$; AD, $P = .0220$). NODDI indicates that hMSC may have preserved intracellular volume fractions (ICVF: day 1, $P = .0086$; day 3, $P = .0021$; day 21, $P = .0383$). Diffusion metrics of hMSC treated animals were comparable to naïve for the external capsule.

Conclusions: NODDI compliments DTI metrics, enhances interpretation of tissue outcome in ischemic stroke following hMSC application, and may be useful in evaluating or predicting therapeutic response.

KEYWORDS
DTI, hMSC, ischemic stroke, mesenchymal stem cells, NODDI

1 | INTRODUCTION

Diffusion weighted imaging (DWI) is a popular method to measure sensitive biomarkers in biological tissue microstructure and infarction in stroke pathology.[1] For quantification of these biomarkers, behavior of water molecules is typically modeled by a Gaussian function to yield the diffusion tensor. Diffusion tensor imaging (DTI) provides directionally dependent quantifications of mean diffusivity (MD) and fractional anisotropy (FA)[2] associated with hindered diffusion under the assumption of a Gaussian fit, whereas restricted diffusion may be modeled differently.[3] Although DTI provides meaningful metrics, the basic imaging protocols are conducted with low b values (0-1500 s/mm^2), and cannot probe microstructures that induce a non-Gaussian water displacement impacted by restricted environments.[4,5] FA shows changes in relative water diffusion directionality but cannot elucidate the primary reasons for such alterations, which may be attributable to distribution, density and orientation of neurites, among other microstructures.[6]

To quantify more specific biomarkers, Neurite Orientation Dispersion and Density Imaging (NODDI)[7] has become a popular extension of DTI. NODDI uses a normalized diffusion signal described by intracellular, extracellular and CSF structural compartments. NODDI models spherical and cylindrical (ball and stick) geometric functions to identify hindered (extra-neurite) and restricted (glial and axonal projections) diffusion[7] as well as their orientations. These measures have been validated with histology,[8] and the model has been applied to various pathologies.[9,10] Incidence of stroke results in diffusivity inhomogeneities due to ischemic hyperintensity,[11,12] which makes DWI an important method in stroke evaluation. NODDI expands on DWI measurements in ischemia, as NODDI indices may compliment FA measurements, highlighting anisotropic changes in neural structures potentially being caused by changes in neurite density or orientation dispersion,[13] and may even be a predictor of outcomes after stroke incidence.[14,15] Additionally, the intracellular volume fraction (ICVF) attained from NODDI may provide a marker for cellular swelling in the context of stroke.

Human mesenchymal stem cells (hMSC) provide therapeutic benefit following neurological damage and have been shown to be a viable approach for mitigating acute and chronic injury following ischemic stroke.[16] Specifically, hMSC have been observed to differentiate into neural and glial proliferates,[17,18] induce angiogenesis,[19,20] cause elevated levels of vascular endothelial growth factor (VEGF), as well as correlate with improved functional and neurological behavior[21-23] in rodent models. Although stem cells are popular in these therapeutic studies, the MR focus of these studies has yet to be tested with higher-order diffusion modeling. Indeed, DTI metric assessments do describe recovery after stem cell intervention in ischemia and their impacts on preventing or mediating reductions in diffusivty[24] and directionality[25] compared to controls, but do not sufficiently characterize or estimate structural and morphological changes that are more specific to microstructure. As such, this study applies therapeutic hMSC to a rodent stroke model and assesses their efficacy in white and gray matter by comparison of DTI and NODDI metrics for the first time. We hypothesize that NODDI will be able to explain physiological changes quantified by DTI via means of intracellular swelling and orientation disruptions in the context of a cell based therapeutic.

2 | METHODS

2.1 | Cell model

Adhering to the NIH Guidelines for Human Stem Cell Research,[26] only adult hMSC were used in this study, as provided by the Tulane Center for Stem Cell Research and Regenerative Medicine. Cells were expanded on tissue culture plates (TCPs) with modified Eagle's medium (α-MEM) (Invitrogen, Grand Island, NY) supplemented with 10% fetal bovine serum (FBS) (Atlanta Biologicals, Lawerenceville, GA) and maintained in an incubator with 95% air (with 20% O_2) 5.0% CO_2 at 37.0°C. The cells in this work are often referred to as 2D hMSC to reflect the two-dimensional culture conditions of the TCP on which cells were expanded.

After in vitro assessment was finished, hMSC were prepared for *in vivo* transplantation. 2D hMSC were cultured to P5, and then labeled with 7.47-μg Fe/mL of micron-sized particles of iron oxide (MPIO) for 12-h prior to *in vivo* transplantation, as in previous studies.[27-29] Immediately prior to injection, the labeled hMSC were washed and suspended in 50-μL phosphate buffered saline (PBS).

2.2 | Animal model

All work has been conducted in accordance with the FSU Institutional Animal Care and Use Committee. All animal experiments comply with the US National Institutes of Health Guide for the Care and Use of Laboratory Animals (NIH Publications No. 8023, revised 1978) as approved and performed. Surgical procedures followed previous method.[28] All animal experiments were conducted in compliance with the Institutional Animal Care and Use Committee at Florida State University and carried out in accordance with the US NIH Guide for the Care and Use of Laboratory Animals (NIH Publications, No. 8023, 1978 revision). Transient middle cerebral arterial occlusion (MCAO) was performed on male Sprague Dawley rats (~200-240 g; Envigo, Indianapolis, IN) for 1 h.[30,31] To occlude the middle cerebral artery (MCA) effectively, a filament (Doccol Corp., Sharon, MA) was placed into the external carotid artery and guided 1.9 cm

through the left internal carotid artery (ICA) toward the MCA. Using the same ICA, rats received an intra-arterial (IA) injection of 1 million hMSC (N = 5) suspended in 50-μL PBS, or control injections of 50-μL PBS (N = 6) immediately after filament removal. Prior to and during surgical procedures, rats were anesthetized with 5% isoflurane in 100% O_2 and maintained between 1% and 3% isoflurane until completion of the operation. For all animals, bupivacaine was administered as a pre-operative analgesic, and buprenorphine was administered as a post-operative analgesic followed by PBS for rehydration. Post-surgical recovery was conducted in an incubation chamber before finally returning to home cages. Additional buprenorphine and PBS were administered daily following surgery on a case-by-case basis determined by weight loss.

2.3 | In vivo MR techniques

All *in vivo* imaging was conducted with the 21.1T ultra-widebore magnet at the National High Magnetic Field Laboratory[32] in Tallahassee, FL. Rats were anesthetized with 5% isoflurane, and subsequently loaded into a linear $^{1}H/^{23}Na$ birdcage coil tuned to 900 MHz for proton scanning, and maintained between 1% and 3% isoflurane. The imaging system has a Bruker Avance III accompanied by ParaVision 6.0.1 (Resonance Research, Inc, Billerica, MA) and respiratory triggering (Model 1025MR, Small Animal Instruments, Inc., NY). All imaging was conducted on days 1, 3, 7 and 21 post-MCAO/injection.

Localizer images were acquired with a ^{1}H fast spin echo (FSE) sequence for initial visualization of the brain in the axial, sagittal and coronal planes. Confirmation of hMSC injection was assessed visually with fast low-angle shot (FLASH) sequence, echo time/repetition time (TE/TR) = 4/1000 ms, resolution = 50 × 50 × 1000 μm, 31 slices and scan time of 10 min.

The diffusion protocol of this study used a four-segment echo planar imaging (EPI) sequence with 4 shells b = (0, 1000, 2000, 3000 s/mm^2), 20 directions applied to the 1000- and 2000-s/mm^2 shells, and 30 directions applied to the 3000-s/mm^2 shell. Four averages were used per image to overcome decreased signal at higher b values with TE/TR = 23.5/4000 ms, resolution = 200 × 200 × 1000 μm, 31 slices and scan time of 78 min plus respiratory trigger. Saturation bands were included to nullify signal outside of the brain.

2.4 | MR data analysis

DTI maps were processed using all b values with DiPy[33] to attain mean, axial, and radial diffusivities (MD, AD, RD, respectively) and FA. All b values were used as this approach reduced variability compared to single-shell analysis and did not influence longitudinal trends. NODDI processing was conducted in MATLAB using the code provided by the original authors[7] to analyze ICVF and orientation dispersion index (ODI). The isotropic volume fraction (V_{iso}) from NODDI modeling, probing the CSF compartment, also was calculated and is presented in Supporting Information Figure S1, which is available online. It should be noted that V_{iso} is reported to have low reproducibility compared to ICVF and ODI in high-field MRI studies of the rat brain with limited sample sizes.[34] Resultant maps from day 1-21 were segmented in AMIRA 3D (Thermo Fisher Scientific, Waltham, MA), with external capsule and striatum region of interest (ROI) manually drawn to address longitudinal and group differences. A radiological reader, different from the individual performing behavioral characterization, drew ROI on non-diffusion-weighted images that were superimposed on diffusion metric maps. Anatomical segmentation was performed in reference to a Sprague Dawley rat brain atlas.[35]

2.5 | Behavioral tests

Behavior tests were conducted on days 0 (baseline), 3, 7, 14, and 21. Asymmetric, locomotor, and anxiety behavioral assessment were performed. The elevated plus maze (EPM) was used for locomotion and anxiety. The EPM consisted of a central area (8.5 × 8.5 cm) connected to two open arms (50 × 8.5 cm) and two closed arms (50 × 8.5 cm) placed in a plus-shape structure and elevated 50 cm above the floor. Animals were placed in the central area of the maze and were recorded by video-tracking camera during a 5-min session. Locomotion was assessed by total distance traveled in the EPM during the session, and anxiety was tested by total amount of time in open versus closed arms, as well as total entries into open versus closed arms.

For asymmetry, the cylinder test[36,37] was used to indicate forelimb preference. Rodents were placed into a vertical cylinder for 10-min, and total forepaw touches against the cylinder wall were recorded with a camera. Scores were calculated as follows:

$$\text{Limb Use Asymmetry Score} = \frac{I}{I+C+B} - \frac{C}{I+C+B}, \quad (1)$$

where I is total ipsilateral forelimb use, C is contralateral forelimb use, and B is use of both forepaws. A score that deviates from zero signifies forelimb preference. Total limb use ($I + C + B$) was calculated as a measure of activity.

To assess weakness post-MCAO, animals underwent a forelimb strength test on their impaired forelimbs. Tests were conducted by holding the rats in a firm but gently vertical position to restrict movement, and gently pushing their forelimb approximately 45 degrees outward. They then were given scores between 0 and 3, with 0 indicating normal strength and resistance during the push, and 3 indicating essentially no

strength or resistance whatsoever. All testing was performed by a qualified individual blinded to the groups.

2.6 | Statistical analysis

Statistical analysis was conducted with JMP 14 software for Windows (SAS Institute, Cary, NC). A mixed model for repeated measures ($P < .05$) was used to test differences between groups between days and longitudinal changes within groups by means of a Tukey's post-hoc test ($P < .05$). Pearson's correlation coefficients were calculated between MRI and behavioral measures within each matching time point of data collection to determine if correlations or unique trends existed between diffusional values and functional outcomes.

3 | RESULTS

In contrast to rats that received PBS (Figure 1A), rats that received 2D hMSC (Figure 1B) display black voids in the ischemic hemisphere resulting from contrast of MPIO-labeled hMSC. Previous work has shown that labeled hMSC target the ischemic lesion but are retained only for a limited number of days, with over 50% reduction in hMSC-related contrast by day 7 post-injection and MCAO.[27] After determination of successful IA delivery of hMSC, regional comparisons of DTI and NODDI metrics were made. It should be noted that the presence of MPIO contrast in brain tissue at the early time points for the hMSC group might be considered to influence diffusion signals. However, for spin-echo acquisitions at 21.1T, recent studies have demonstrated that the presence of MPIO-labeled cells has minimal impact on the absolute diffusion coefficient.[38,39] Furthermore, the presence of MPIO contrast significantly decreases within the first 3 days, reaching a greater than 65% reduction by day 7.[27] Only animals with visually confirmed hMSC injections were included in the 2D hMSC group for the full study.

3.1 | Diffusion metrics in the external capsule and striatum

3.1.1 | Ipsilateral external capsule

MCAO PBS-injected controls had significantly lower MD and AD (Figure 2A,B) on day 1 relative to naïve ($P = .0106$) and 2D hMSC ($P = .0406$) cohorts. On day 3, PBS group diffusivities were still significantly lower than the hMSC group ($P = .0015$) but were close to naïve. Both axial and radial diffusivities followed similar trends for each group longitudinally, highlighted by similar FA (Figure 2C) values between cell and control treatment animals. Conversely, cell swelling (ICVF, Figure 3A) is only elevated following the ischemic event after PBS was injected. PBS ICVF was significantly higher than naïve at day 1 ($P = .0125$), and significantly higher than the hMSC group on days 1 ($P = .0086$), 3 ($P = .0021$) and 21 ($P = .0383$). ODI (Figure 3B) in the external capsule remains unchanged following hMSC treatment but is slightly elevated after PBS injection. This elevation is significant on day 21 ($P = .0421$). Contralateral data did not deviate from naïve across any metrics. Severity within ischemic hemispheres was evaluated by ipsilateral-to-contralateral comparisons. In the external capsule, PBS-injected animals displayed significant hemispheric differences on day 1 (MD, $P = .0240$; AD, $P = .0461$; RD, $P = .0226$). hMSC-treated animals had significant differences on days 1 (RD, $P = .0497$; FA, $P = .0265$) and 3 (AD, $P = .018$; ICVF, $P = .0265$).

3.1.2 | Ipsilateral striatum

For PBS and hMSC injections, DTI metrics (Figure 2) had nearly identical trends and values over the entire time course, although cell-treated animals did (on average) reach naïve diffusivity levels quicker than PBS-injected. Likewise, trends in ICVF (Figure 3A) and ODI (Figure 3B) recovery also were

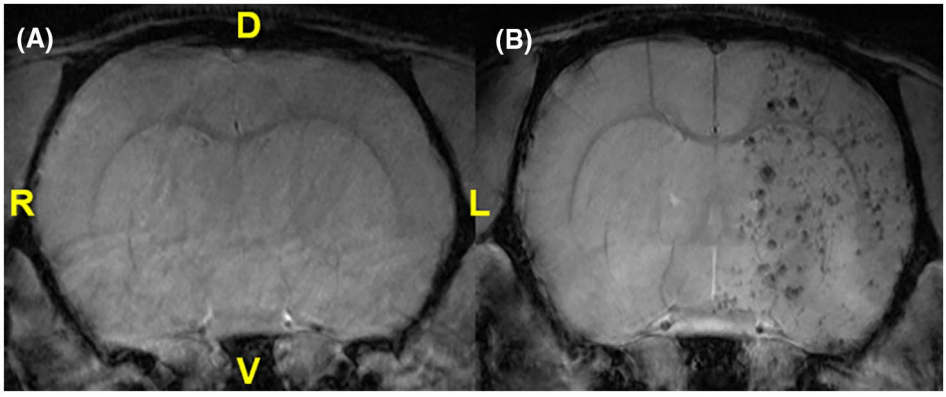

FIGURE 1 FLASH images of *in vivo* rat brains following PBS (A) or 2D hMSC (B) administration. Anatomical references are provided for dorsal (D), ventral (V), left (L), and right (R) orientations, with the left anatomical hemisphere corresponding to the ipsilateral (ischemic) side and showing decoration by MPIO-labeled 2D hMSC injected intra-arterially

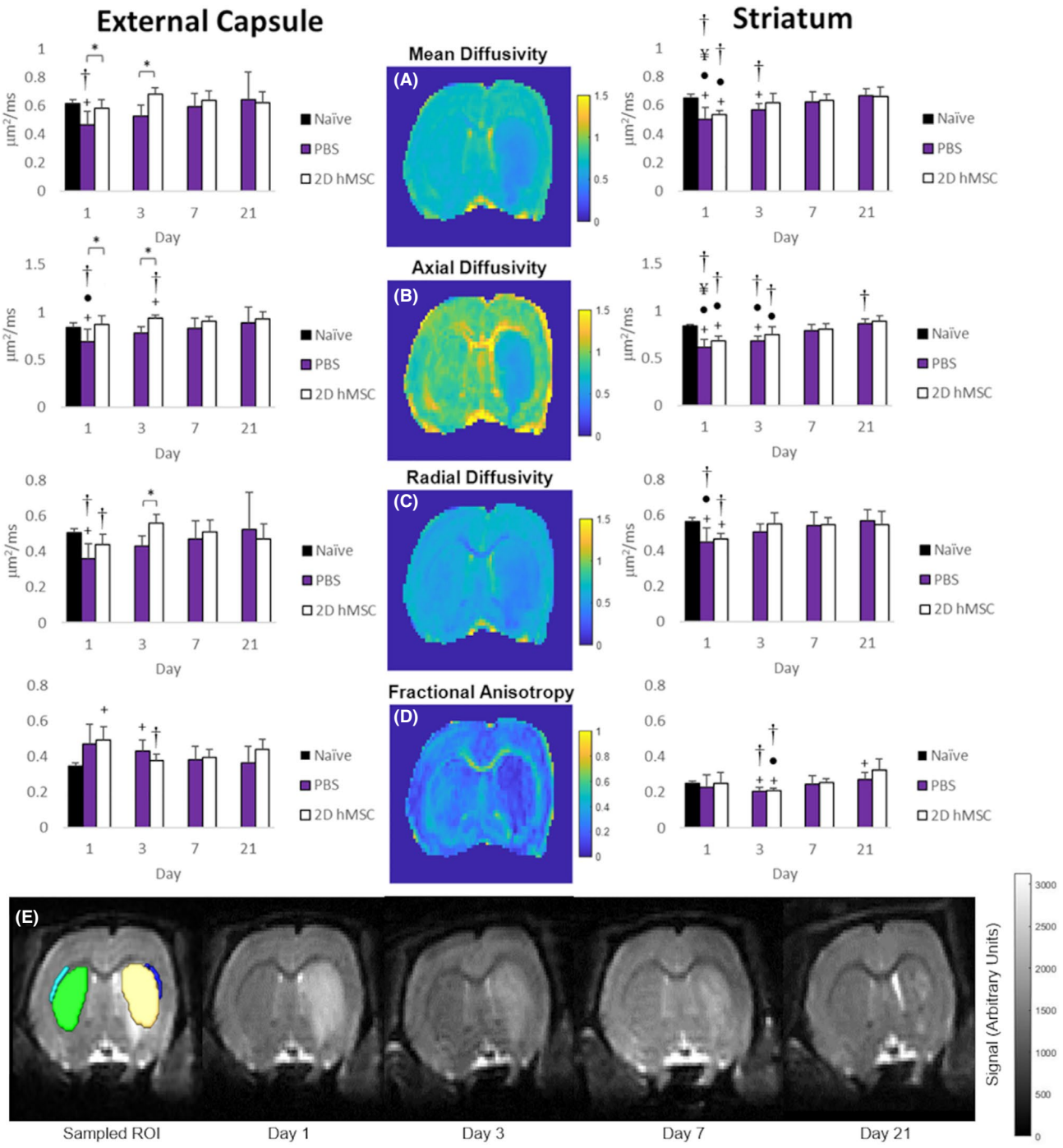

FIGURE 2 MD(A), AD(B), RD (C), and FA (D) for PBS and 2D hMSC-treated animals in the external capsule (left) and striatum (right) column. E, Sample T_2W images of ROI drawn in ipsilateral external capsule (dark blue) and striatum (yellow), as well as contralateral external capsule (light blue), striatum (green). Data displayed as means and standard deviations across all specimens in each group. * = sig diff between treatment groups, + = sig diff between treatment group & naïve, #, ¥, and ● = sig diff between data on labeled time point and day 3, 7, and 21, respectively. † = sig diff between ipsilateral and contralateral hemispheres. $P < .05$. DTI metric maps (center) correspond to day 1 of a representative rat that received 2D hMSC treatment after MCAO. E, T_2W images represent this same rat at each time point

similar between groups: an increase at the initial time point compared to naïve followed by a gradual decrease. It should be noted that the hMSC group ICVF was closest to naïve levels at each time point, and only the PBS-injected group was significantly higher than naïve on days 1 ($P = .0041$) and 3 ($P = .0156$). Each groups' ODI were elevated significantly over naïve, but only hMSC-treated animals recovered to normal levels by day 21 ($P = .0294$).

Striatal contralateral data were not statistically different from naïve. Comparing ipsilateral and contralateral striatum, the PBS group had significant differences on day 1 (MD, $P = .0010$; AD, $P = .0001$; RD, $P = .0060$; ICVF, $P = .0275$;

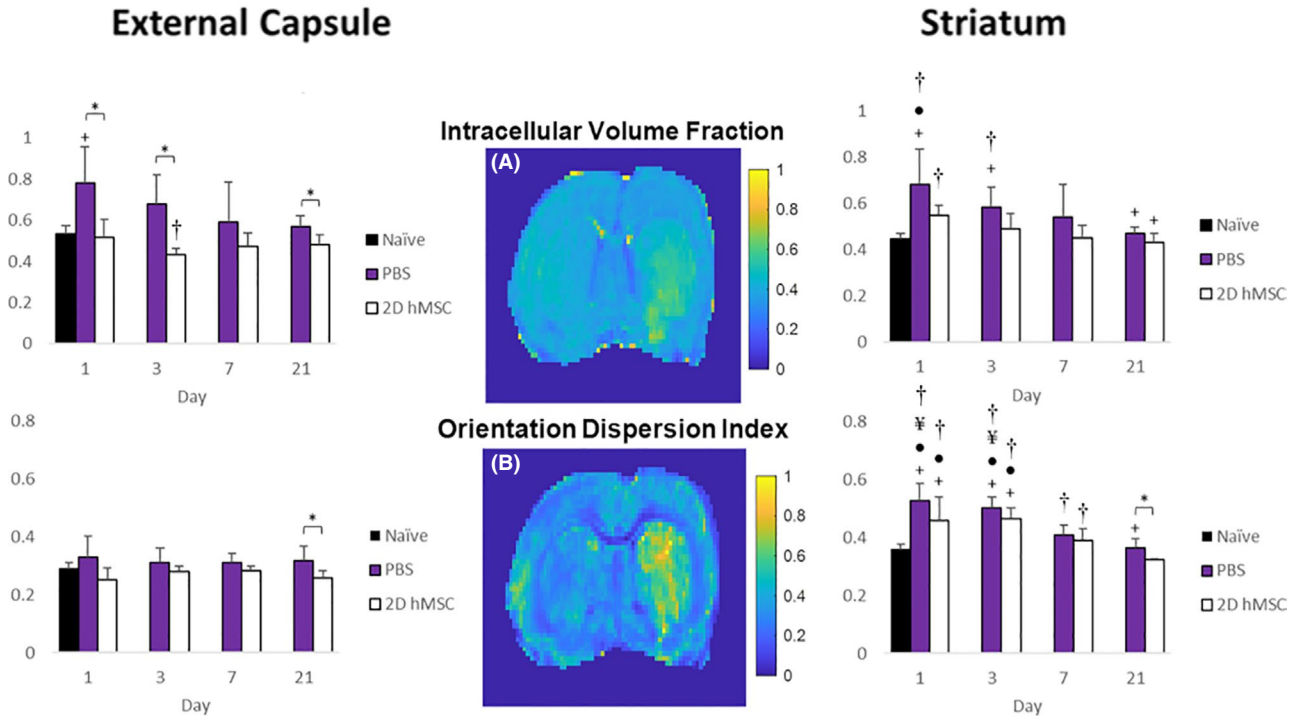

FIGURE 3 ICVF (A) and ODI (B) for PBS and 2D hMSC-treated animals in the external capsule and striatum. Data displayed as means and standard deviations across all specimens in each group. * = sig diff between treatment groups, + = sig diff between treatment group & naïve, #, ¥, and ● = sig diff between data on labeled time point and day 3, 7, and 21, respectively. † = sig diff between ipsilateral and contralateral hemispheres. $P < .05$. NODDI metric maps (center) correspond to day 1 of a representative rat that received 2D hMSC treatment after MCAO

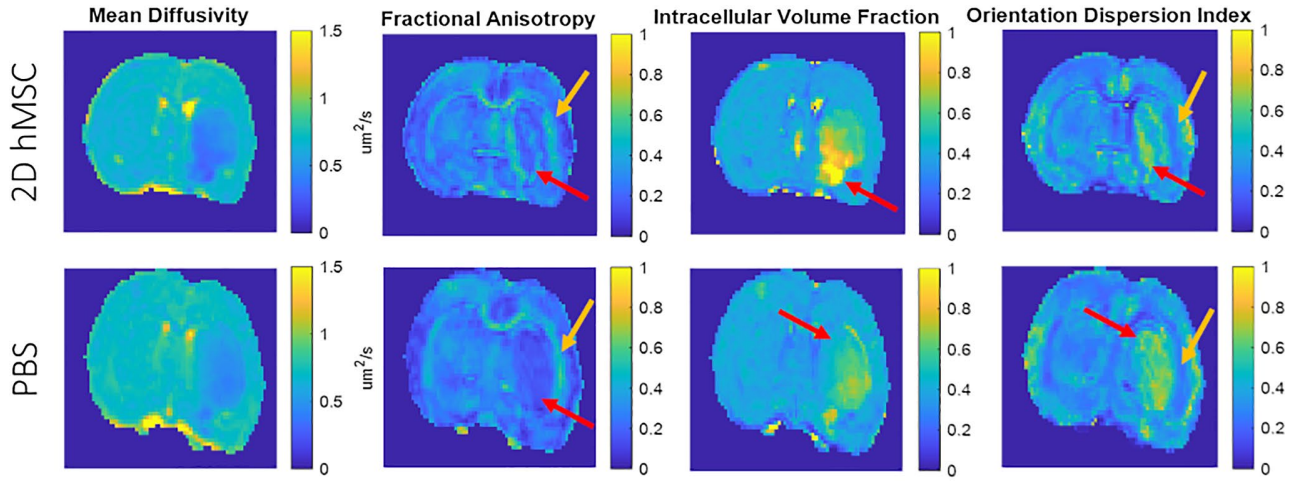

FIGURE 4 Visual differences observed between DTI and NODDI metrics. Images shown from sample PBS and 2D hMSC-injected rats on day 1. Red arrows indicate inhomogeneous regions within the lesion that appear distinct compared to other regions within the same animal, while gold arrows indicate apparent differences at the interface between white and gray matter

ODI, $P = .0001$), day 3 (MD, $P = .0083$; AD, $P = .0002$; FA, $P = .0003$; ICVF, $P = .0211$; ODI, $P = .0001$), day 7 (ODI, $P = .0021$) and day 21 (AD, $P = .0226$). Hemispheric differences after hMSC treatment were on day 1 (MD, $P = .0001$; AD, $P = .0014$; RD, $P = .0004$; ICVF, $P = .0001$; ODI, $P = .0288$), day 3 (AD, $P = .0377$; FA, $P = .0127$; ODI, $P = .0022$), and day 7 (ODI, $P = .0428$). Inhomogeneities within the ischemic lesion that typically dominate the striatal region are seen in Figure 4. These inhomogeneities appear to be most prominent in the FA, ICVF, and ODI metrics and are relatively distinct from one another. They also may appear regardless of treatment group.

3.2 | Behavior

3.2.1 | Elevated plus maze

For the EPM (Figure 5), rats were tracked for number of entries into closed or open arms, time spent in closed or open arms, and total distance traveled within 5 min. On average, rats treated with hMSC spent more time in open arms of the EPM relative to their baseline measures. This metric (Figure 5B,C) reached significance on day 3 between groups (P = .0360) and longitudinally within the hMSC group compared to other time points (day 1-3 P = .0028; day 3-7 P = .0190; day 3-14 P =0.0155; day 3-21 P = .0029). No trends or significance were found concerning the open or closed arm entries, either between groups or longitudinally. Relative to baseline distance traveled, the hMSC group traveled a greater distance on average in the EPM compared to the PBS group, but not significantly (Figure 5D).

3.2.2 | Cylinder test

The cylinder test (Figure 6) was used to assess limb preference asymmetry and overall activity by assessing the total number of wall touches in the cylinder by individual rats over ten minutes. By day 21, asymmetry is lowest on average for hMSC-treated animals, although with large SDs that are apparent across all time points for all groups. In contrast, the total number of wall touches relative to baseline is less variable: hMSC-treated animals had an on average a higher number of wall touches at each time point post-MCAO compared to PBS and a significant number of touches as a marker of activity on day 14 (P = .0137).

3.2.3 | Forelimb strength

Forelimb strength (Figure 7) was impaired severely in the PBS-injected animals. On day 3, forelimb weakness in the PBS group was significantly higher than the hMSC-treated group (P = .0152). By day 7, both groups had similar weakness scores, with hMSC-treated animals having a lower score on average. Only the PBS group recorded weakness scores at each time point post-MCAO significantly higher than baseline. The hMSC group never significantly deviated from baseline.

3.2.4 | Correlations between MR and behavior

Pearson's coefficients were calculated to determine potential correlations between MR metrics of diffusion and behavioral outcomes on days with overlapping data. Although animal numbers are low for behavioral characterization given their dual use for MRI scans, the most interesting correlations are shown longitudinally for diffusional metrics with differences between the treatment groups in Supporting Information Figures S2 and S3.

4 | DISCUSSION

4.1 | 2D hMSC have a dramatic effect on white matter integrity

As there is more statistical significance between groups in the external capsule for each metric, it appears that 2D hMSC effectively reduce the restrictive effects

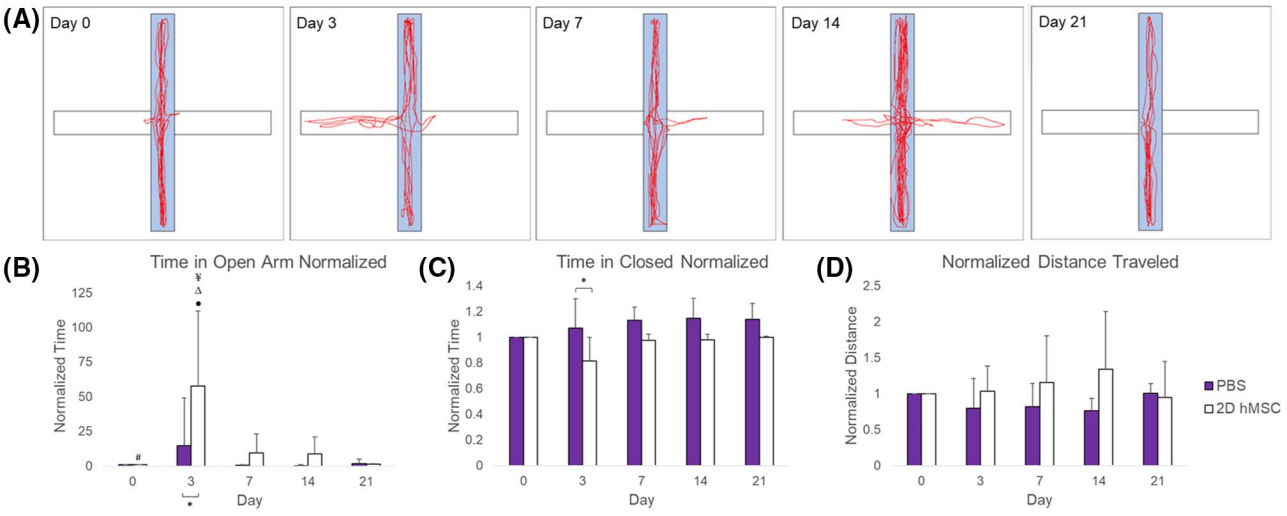

FIGURE 5 EPM results: Sample diagram of hMSC-treated rat behavior in EPM over 21 days (A), time spent in open arm (B), time spent in closed arm (C),and distance traveled (D), all normalized to baseline measures. Data displayed as means and standard deviations across all specimens in each group. * = sig diff between treatment groups, + = sig diff between treatment group & naïve, #, ¥, Δ, and ● = sig diff between data on labeled time point and day 3, 7, 14, and 21, respectively. $P < .05$

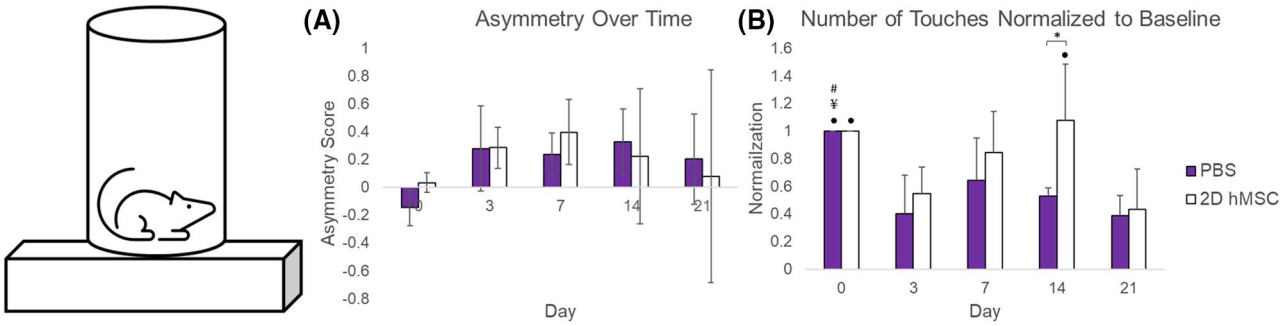

FIGURE 6 Cylinder test results: Raw asymmetry scores over time (A) and number of wall touches normalized to baseline (B). Data displayed as means and standard deviations across all specimens in each group. * = sig diff between treatment groups, + = sig diff between treatment group and naïve, #, ¥, Δ, and ● = sig diff between data on labeled time point and day 3, 7, 14, and 21, respectively. $P < .05$

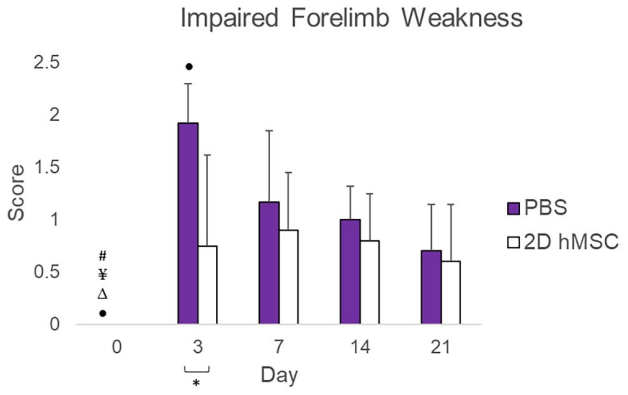

FIGURE 7 Impaired forelimb weakness scores, normalized to baseline (day 0). Data displayed as means and standard deviations across all specimens in each group. * = sig diff between treatment groups, + = sig diff between treatment group & naïve, #, ¥, Δ, and ● = sig diff between data on labeled time point and day 3, 7, 14, and 21, respectively. $P < .05$

of ischemic attack compared to PBS controls in both axial and radial directions for the entire time course. Considering NODDI data, this protective impact seems largely due to the preservation of intracellular volumes and neurite orientations following hMSC administration. In sharp contrast, PBS-injected animals suffered from extreme restrictions due to white matter cell swelling (via ICVF), with minor disruptions in orientation dispersion. Clear cell swelling and orientational differences are still evident when comparing groups with NODDI at day 21. The combination of altered DTI with NODDI metrics seems to be evident for white matter restrictions initially, but NODDI alterations also may describe neurite changes up to day 21 unresolved by DTI (Figure 3). These trends could imply that (1) moderate cell swelling and disruption of orientation could be permanent or chronic to some degree in non-hMSC-treated animals and (2) late-term elevated ICVF and ODI (when evident) may be more sensitive and decoupled from DTI metrics that are weighted toward extracellular restriction.

As most metrics at least return close to naïve white matter levels at baseline, it appears all diffusion metrics recover in some capacity over 21 days. Acute application of hMSC may streamline recovery by reducing the overall effects of initial ischemia, returning diffusional metrics to baseline more rapidly. Trends for directional diffusivities indicate both the axial and radial directions in the external capsule are equally affected under ischemic insult and with hMSC treatment, ie, hMSC mediated impacts or untreated ischemic evolution although different are not directionally dependent in this white matter structure. Longitudinally and between groups, contralateral tissue had no significant differences across metrics. Ipsilateral-to-contralateral comparisons show more instances of relative hemispheric DTI changes after PBS injection on day 1, with limited hemispheric changes after hMSC treatment. Although the PBS group had significantly higher ICVF on each day, the lack of hemispheric differences may be due to ipsilateral standard deviations. Localization of the ischemic lesion and hMSC distribution within the lesion are likely the cause of isolated effects within ipsilateral tissue as opposed to contralateral.

MRI studies that use cell therapies in the ischemic stroke model are largely limited to DTI metrics. Previously, a murine study found that neural stem cell extracellular vesicle application did not show differences in FA between treated versus control groups, likely due to the minimal white matter content in rodents.[40] In contrast, adipose-derived MSC applied intravenously in a rat model of ischemic stroke in a separate study showed elevated axial diffusivity in subcortical white matter at 28 d post-ischemic insult.[24] The results of Figure 2 display a much earlier difference in the external capsule AD and MD on days 1 and 3 between groups, with the hMSC group not significantly different from naïve. Differences in the time course of these changes from the work of Otero-Ortega et al[24] may result from differences in the ischemic models, injection routes, treatment times post-ischemia, types of MSC, or a combination of the above. In a porcine model, significant differences in white matter FA have been observed between treatment and non-treatment

groups long-term when using neural stem cell-derived extracellular vesicles[25] and induced pluripotent stem cell-derived neural stem cells,[41] which has been extended to rodent models for which FA alterations correlated with myelination immunohistochemistry.[42] Indeed, FA in the current study was on average higher in hMSC-treated animals by day 21 (although not significantly), which also has been observed in ischemic mice treated with MSC-derived exosomes[43] by day 14. Morphological differences in rat brain tissue after stroke has been reported previously using NODDI metrics, which were correlated to histology that confirmed neuronal swelling, bending and distortions in the short-term,[44] although not with stem cell application. A suspected reason for this swelling could be inflammatory and glial infiltration into the extra-neurite space,[14] and MSC application has been reported to attenuate this type of inflammatory response.[45] Although trends are apparent and V_{iso} (Supporting Information Figure S1) has been suggested as a means of quantifying potential inflammatory activity, variability is too high to achieve statistical significance for this biomarker, which has been questioned previously in NODDI rodent studies with respect to the reproducibility of V_{iso}.[34] Based on previous and current evidence, stem cell treatments here resulted in positive white matter recovery or preservation of diffusivities.

To date, NODDI has not been as thoroughly applied to the study of ischemic stroke. However, NODDI has been shown previously to offer increased sensitivity compared to DTI in humans after ischemic stroke,[46] particularly with respect to white matter microstructure.[13] Even though white matter abnormalities and recovery are more obvious, characterization of the lesion itself with higher-order diffusion models may probe a fuller extent of resulting damage.[47] In this study, ICVF and ODI support and enhance the interpretation of standard DTI data, adding sensitive metrics to white matter swelling and recovery resulting from stem cell therapy. Based on the literature, these metrics also may provide biometrics for inflammatory response that are altered by hMSC. This approach constitutes the first time NODDI metrics have been used to evaluate the efficacy of such a stroke treatment.

4.2 | Stem cells have a moderate effect on gray matter

In contrast to the external capsule, the striatum was impacted in all groups. On average, the directional diffusivities of hMSC-treated animals were less drastically affected. There was no significance between groups for DTI metrics, but hMSC-treated animals did appear to reach naïve levels faster (by day 3) than PBS. ICVF indicated that cell swelling was typically lower following hMSC application, but the variance in ICVF in the PBS control group was large enough to undercut significance with treatment. Although ischemic attack drastically increases orientation dispersion of the neurite model,[46] hMSC effectively return ODI to naïve levels by day 21, whereas PBS does not, which may be the result of inflammatory response altered by the potential glial and remodeling mechanisms mentioned previously.[42,48] As was the case with the external capsule, DTI metrics recover by day 21 in a similar fashion, but ICVF and ODI maintain differences between groups in some capacity throughout the time course, reflecting potentially altered recovery mechanisms as a result of hMSC therapy that are made evident by NODDI. Striatal hemispheric differences are extensive for both groups, with PBS injections displaying more metric and longitudinal differences and variance. Striatal brain tissue retains more similarity to the non-ischemic hemisphere with respect to restriction and structural integrity after hMSC treatment, supporting the protective effects of hMSC in gray matter over the more variable findings with PBS injection.

Striatal results are in sharp contrast to the external capsule and display the differential recovery mechanisms between white and gray matter in a therapeutic context. It is clear that hMSC prevent increased restriction, ICVF-delineated cell swelling and orientation alterations compared to control treatment in white matter, while gray matter shows some similar trends, on average a lower response to ischemic attack after hMSC application, but without distinct preservation of neurite cell volume fraction or orientation. For both gray and white matter, it seems that all metrics can describe physiological manifestations adequately within the first 3 days and provide supportive context. As structural differences and abnormalities beyond this timeframe are only identified by NODDI metrics in both tissue types, the use of the multiple diffusion metrics assessed here provides a clearer picture of therapeutic response after ischemic stroke while highlighting the specific usefulness of certain diffusion metrics on a temporal basis.

Last, as an important area of ischemic stroke imaging is identification of lesion extent and severity, hyperintense regions at the lesion periphery or penumbra may be beneficial in prognosis and treatment assessment in a clinical context. Differential lesion heterogeneity as displayed by maps of both DTI and NODDI metrics (Figure 4) may represent pathological issues or therapeutic impacts. Heterogeneity is also observed on representative biomarker maps (Figures 3 and 4) with respect to the ipsilateral interface of the striatal and external capsule, potentially even more generally at the gray and white matter boundary. Although the exact mechanisms underlying specific heterogeneity may not be fully understood, identification of heterogeneity still may provide greater context to regional physiological impacts of pathology or treatment that may prove therapeutically relevant. Some animals in this study had clear indications of regional abnormalities that were identified by some diffusion metrics

but unremarkable with others. These heterogeneities were not unique to individual animals or groups.

4.3 | Behavior assessments support MR findings

In a similar fashion to DTI and NODDI assessments, activity in the EPM shows major differences between groups, supporting significant diffusion findings on day 3. As this is most prominent for the time spent in the open arm of the EPM, exploratory behavior 3 days post-MCAO may be indicative of early physiological recovery identified by MR findings. In line with EPM, the forelimb strength of both groups displays a similar pattern on day 3, with PBS-injected animals displaying drastically weaker forelimb strength. As forelimb strength is similar between groups after day 3, the weakness in forelimb strength of the PBS group may explain partially why these animals are less exploratory than the hMSC group. In support of this finding, functional and behavioral recovery within 3 days has been reported in mice[49] and rats[50] following MSC or MSC-derived treatment. Additionally, 2D hMSC-treated animals appear to be more active than controls when quantifying the number of forepaw touches against the wall of the cylinder on day 14. Although the EPM and cylinder test show significance at different time points, there is a clear pattern of elevated physical activity following hMSC application out to at least 2 wk post-MCAO. Comparable to cylinder test wall touches here, behavior changes using the cylinder test have been observed following early phase MSC treatment of ischemic stroke in rats with high significance around day 14,[51] as have motor ability assessments in a similar context.[52] Neurological and functional severity scores also have been reported to be improved significantly following stem cell application compared to controls approximately 2 wk following application.[53,54] As such, DTI and NODDI data suggest that hMSC-mediated behavioral deviations may be matched or predicted in ischemic stroke by higher order diffusion imaging techniques and models.

DTI metrics and behavioral outcome correlations display progressively positive correlations for hMSC treatment, reaching the highest positive correlations (aside from FA) at day 21 in contrast to highly negative day 21 correlations for PBS (Supporting Information Figure S2). For NODDI-behavior correlations (Supporting Information Figure S3), ICVF had weak correlations on each day assessed in the external capsule, with stronger albeit negative correlations for PBS in the striatum. These correlations potentially reflect impacts of striatal swelling on day 21 behavior. External capsule ODI correlations with behavior were positive and highly so ($r > 0.5$) for hMSC treatment on days 3 and 21 but negative for PBS correlations ($r < -0.5$) on days 3 and 7. Striatal ODI correlations progressively become more negative for the PBS group. It is plausible that the typically positive correlations between diffusion biomarkers and behavioral results observed for the hMSC group may further support stem cell induced recovery as it relates to functional outcome.

4.4 | Limitations

Although efforts have been made to reduce overall study limitations be means of the experimental design, certain limitations persist. There are immense disparities in MR study designs in the literature. As ischemic stroke research is widespread, the degrees of freedom between studies can be enormous with respect to animal model, ischemic injury, and administration route of cell therapy, as well as the kind of cells and timing of their application. Because of these variations, direct comparisons can be difficult to make. In the current study, 2D cultured bone-marrow-derived hMSC were applied intra-arterially acutely and immediately following the release of transient middle cerebral occlusion. As a result, these studies may represent a best-case scenario for the application of cell therapy in the treatment of stroke, which may be difficult to replicate in a clinical setting. Future studies can and will evaluate other time courses of stem cell delivery that more closely resemble clinical conditions.

Future efforts also will seek to evaluate diffusion kurtosis[55] to further enhance treatment interpretations and recovery of ischemic stroke. As kurtosis (curvature of the path of diffusion) could support additional factors present in the extracellular space, such as debris from necrosis, demyelination,[56] astrocytic scarring,[57] and neurite beading,[58] it may be a worthwhile pursuit. Histology also may be desirable to identify specific cellular responses, neurogenesis, and recovery mechanisms.

5 | CONCLUSIONS

This study has evaluated the effectiveness of 2D hMSC in the treatment of ischemic stroke by using diffusional metrics in the form of DTI and NODDI, and the novelty of NODDI in evaluating cellular therapeutics is established. This study is the first work to judge the efficacy of a cell therapy in an ischemic stroke model using NODDI. In particular, ICVF reflects enhanced therapeutic efficacy and lesion heterogeneity, potentially extending the scope of interpretation beyond the prognostic value of DTI. NODDI strengthens the understanding of white matter in the ischemic stroke model under the influence of cell therapy, predominantly with the ICVF as a quantitative marker of cell swelling. To a lesser extent, gray matter recovery is further enhanced. Furthermore, NODDI improves interpretation of DTI results and gives context

to the evolution of extracellular restriction in both regions. Behavioral analysis of exploratory behavior, forelimb activity and forelimb weakness support these MR findings, with consistency in significant behavioral time points that mirror DTI and NODDI significance between groups. In addition to diagnostic interpretation, the potential of these techniques to expand clinical applications of NODDI to interpret post-stroke treatments should be evaluated further.

ACKNOWLEDGMENTS

Funding was provided by NIH (RO1-NS102395). The National High Magnetic Field Laboratory and 900 UWB magnet are supported by the National Science Foundation (DMR-1644779) and State of Florida.

DATA AVAILABILITY STATEMENT

All data used in this study was newly acquired. Relevant data used in preparation of this manuscript is available upon request to either the principal or corresponding author via email. In accordance with the National High Magnetic Field Laboratory FAIR Data Management Plan (www.nationalmaglab.org/about/fair-data), data can be made available for access through the NHMFL publication database.

ORCID

Samuel C. Grant https://orcid.org/0000-0001-7738-168X

REFERENCES

1. Moseley ME, Cohen Y, Mintorovitch J, et al. Early detection of regional cerebral ischemia in cats: comparison of diffusion- and T2-weighted MRI and spectroscopy. *Magn Reson Med*. 1990;14:330-346.
2. Basser PJ, Pierpaoli C. Microstructural and physiological features of tissues elucidated by quantitative-diffusion-tensor MRI. *J Magn Reson Ser B*. 1996;111:209-219.
3. Assaf Y, Cohen Y. Assignment of the water slow-diffusing component in the central nervous system using q-space diffusion MRS: implications for fiber tract imaging. *Magn Reson Med*. 2000;43:191-199.
4. Pierpaoli C, Basser PJ. Toward a quantitative assessment of diffusion anisotropy. *Magn Reson Med*. 1996;36:893-906.
5. Pierpaoli C, Jezzard P, Basser PJ, Barnett A, Di Chiro G. Diffusion tensor MR imaging of the human brain. *Radiology*. 1996;201:637-648.
6. Beaulieu C. The biological basis of diffusion anisotropy. In: Johansen-Berg H, Behrens TEJ, eds. *Diffusion MRI*. Cambridge, MA: Academic Press; 2009:105-126.
7. Zhang H, Schneider T, Wheeler-Kingshott CA, Alexander DC. NODDI: practical *in vivo* neurite orientation dispersion and density imaging of the human brain. *Neuroimage*. 2012;61:1000-1016.
8. Yi SY, Barnett BR, Torres-Velázquez M, et al. Detecting microglial density with quantitative multi-compartment diffusion MRI. *Front Neurosci*. 2019;13:81.
9. Colgan N, Siow B, O'Callaghan JM, et al. Application of neurite orientation dispersion and density imaging (NODDI) to a tau pathology model of Alzheimer's disease. *Neuroimage*. 2016;125:739-744.
10. Crombe A, Planche V, Raffard G, et al. Deciphering the microstructure of hippocampal subfields with *in vivo* DTI and NODDI: applications to experimental multiple sclerosis. *Neuroimage*. 2018;172:357-368.
11. Eswaradass P, Appireddy R, Evans J, et al. Imaging in acute stroke. *Expert Rev Cardiovasc Ther*. 2016;14:963-975.
12. Yoo AJ, González RG. Clinical applications of diffusion MR imaging for acute ischemic stroke. *Neuroimaging Clin N Am*. 2011;21:51-69.
13. Adluru G, Gur Y, Anderson JS, Richards LG, Adluru N, Dibella EVR. Assessment of white matter microstructure in stroke patients using NODDI. *Conf Proc IEEE Eng Med Biol Soc*. 2014;2014:742-745.
14. Hodgson K, Adluru G, Richards LG, et al. Predicting motor outcomes in stroke patients using diffusion spectrum MRI microstructural measures. *Front Neurol*. 2019;10:1-9.
15. Ohki A, Saito S, Hata J, Okano HJ, Higuchi T, Fukuchi K. Neurite orientation dispersion and density imaging for evaluating the severity of neonatal hypoxic-ischemic encephalopathy in rats. *Magn Reson Imaging*. 2019;62:214-219.
16. Wakabayashi K, Nagai A, Sheikh AM, et al. Transplantation of human mesenchymal stem cells promotes functional improvement and increased expression of neurotrophic factors in a rat focal cerebral ischemia model. *J Neurosci Res*. 2009;88 1017-1025.
17. Woodbury D, Schwarz EJ, Prockop DJ, Black IB. Adult rat and human bone marrow stromal cells differentiate into neurons. *J Neurosci Res*. 2000;61:364-370.
18. Kim S, Honmou O, Kato K, et al. Neural differentiation potential of peripheral blood- and bone-marrow-derived precursor cells. *Brain Res*. 2006;1123:27-33.
19. Zacharek A, Chen J, Li A, et al. Angiopoietin1/Tie2 and VEGF/Flk1 induced by MSC treatment amplifies angiogenesis and vascular stabilization after stroke. *J Cereb Blood Flow Metab*. 2007;27:1684-1691.
20. Mora-Lee S, Sirerol-Piquer MS, Gutiérrez-Pérez M, et al. Therapeutic effects of hMAPC and hMSC transplantation after stroke in mice. *PLoS One*. 2012;7:e43683.
21. Li Y, Chen J, Wang L, Lu M, Chopp M. Treatment of stroke in rat with intracarotid administration of marrow stromal cells. *Neurology*. 2001;56:1666-1672.
22. Horita Y, Honmou O, Harada K, Houkin K, Hamada H, Kocsis JD. Intravenous administration of glial cell line-derived neurotrophic factor gene-modified human mesenchymal stem cells protects against injury in a cerebral ischemia model in the adult rat. *J Neurosci Res*. 2006;84:1495-1504.
23. Chen J, Li YI, Wang L, et al. Therapeutic benefit of intravenous administration of bone marrow stromal cells after cerebral ischemia in rats. *Stroke*. 2001;32:1005-1011.
24. Otero-Ortega L, Gutiérrez-Fernández M, Ramos-Cejudo J, et al. White matter injury restoration after stem cell administration in subcortical ischemic stroke. *Stem Cell Res Ther*. 2015;6:1-12.
25. Webb RL, Kaiser EE, Jurgielewicz BJ, et al. Human neural stem cell extracellular vesicles improve recovery in a porcine model of ischemic stroke. *Stroke*. 2018;49:1248-1256.
26. *National Institutes of Health Guidelines for Human Stem Cell Research*. stemcells.nih.gov. https://stemcells.nih.gov/policy/2009-guidelines.htm. Accessed June 5, 2021.

27. Yuan X, Rosenberg JT, Liu Y, Grant SC, Ma T. Aggregation of human mesenchymal stem cells enhances survival and efficacy in stroke treatment. *Cytotherapy*. 2019;21:1033-1048.
28. Rosenberg JT, Sellgren KL, Sachi-Kocher A, et al. Magnetic resonance contrast and biological effects of intracellular superparamagnetic iron oxides on human mesenchymal stem cells with long-term culture and hypoxic exposure. *Cytotherapy*. 2013;15:307-322.
29. Sart S, Bejarano FC, Baird MA, et al. Intracellular labeling of mouse embryonic stem cell–derived neural progenitor aggregates with micron-sized particles of iron oxide. *Cytotherapy*. 2015;17:98-111.
30. Longa E, Weinstein P, Carlson S, Cummins R. Reversible middle cerebral artery occlusion without craniectomy in rats. *Stroke*. 1989;20:84-91.
31. Tajiri N, Dailey T, Metcalf C, et al. *In vivo* animal stroke models: a rationale for rodent and non-human primate models. *Transl Stroke Res*. 2013;4:308-321.
32. Fu R, Brey WW, Shetty K, et al. Ultra-wide bore 900 MHz high-resolution NMR at the national high magnetic field laboratory. *J Magn Reson*. 2005;177:1-8.
33. Garyfallidis E, Brett M, Amirbekian B, et al. Dipy, a library for the analysis of diffusion MRI data. *Front Neuroinform*. 2014;8:1-17.
34. McCunn P, Gilbert KM, Zeman P, et al. Reproducibility of neurite orientation dispersion and density imaging (NODDI) in rats at 9.4 Tesla. *PLoS One*. 2019;14:e0215974.
35. Papp EA, Leergaard TB, Calabrese E, Johnson GA, Bjaalie JG. Waxholm space atlas of the sprague Dawley rat brain. *Neuroimage*. 2014;97:374-386.
36. Schaar KL, Brenneman MM, Savitz SI. Functional assessments in the rodent stroke model. *Exp Transl Stroke Med*. 2010;2:13.
37. Schallert T, Fleming SM, Leasure JL, Tillerson JL, Bland ST. CNS plasticity and assessment of forelimb sensorimotor outcome in unilateral rat models of stroke, cortical ablation, Parkinsonism and spinal cord injury. *Neuropharmacology*. 2000;39:777-787.
38. Leftin A, Rosenberg JT, Yuan X, Ma T, Grant SC, Frydman L. Multiparametric classification of sub-acute ischemic stroke recovery with ultrafast diffusion, 23Na, and MPIO-labeled stem cell MRI at 21.1 T. *NMR Biomed*. 2020;33:e4186.
39. Rosenberg JT, Leftin A, Solomon E, Frydman L, Grant SC. Diffusion-weighted spatiotemporal encoding schemes in the assessment of SPIO-labeled cell therapy for ischemic stroke. In: Proceedings of the ISMRM 23rd Annual Meeting & Exhibition, Toronto, Ontario, Canada. 2015, p. 2144.
40. Webb RL, Kaiser EE, Scoville SL, et al. Human neural stem cell extracellular vesicles improve tissue and functional recovery in the murine thromboembolic stroke model. *Transl Stroke Res*. 2018;9:530-539.
41. Baker EW, Platt SR, Lau VW, et al. Induced pluripotent stem cell-derived neural stem cell therapy enhances recovery in an ischemic stroke pig model. *Sci Rep*. 2017;7:1-15.
42. Jiang Q, Zhang ZG, Ding GL, et al. MRI detects white matter reorganization after neural progenitor cell treatment of stroke. *Neuroimage*. 2006;32:1080-1089.
43. Xu R, Bai Y, Min S, Xu X, Tang T, Ju S. *In vivo* monitoring and assessment of exogenous mesenchymal stem cell-derived exosomes in mice with ischemic stroke by molecular imaging. *Int J Nanomedicine*. 2020;15:9011-9023.
44. Wang Z, Zhu W, Zhang S, Shaghaghi M, Cai K. Neurite orientation dispersion and density imaging of rat brain microstructural changes due to middle cerebral artery occlusion at a 3T MRI. *Curr Med Sci*. 2021;41:167-172.
45. Li YI, Chen J, Zhang CL, et al. Gliosis and brain remodeling after treatment of stroke in rats with marrow stromal cells. *Glia*. 2005;49:407-417.
46. Wang Z, Zhang S, Liu C, et al. A study of neurite orientation dispersion and density imaging in ischemic stroke. *Magn Reson Imaging*. 2019;57:28-33.
47. Bay V, Kjølby BF, Iversen NK, et al. Stroke infarct volume estimation in fixed tissue: comparison of diffusion kurtosis imaging to diffusion weighted imaging and histology in a rodent MCAO model. *PLoS One*. 2018;13:e0196161.
48. Anderova M, Vorisek I, Pivonkova H, et al. Cell death/proliferation and alterations in glial morphology contribute to changes in diffusivity in the rat hippocampus after hypoxia-ischemia. *J Cereb Blood Flow Metab*. 2011;31:894-907.
49. Sammali E, Alia C, Vegliante G, et al. Intravenous infusion of human bone marrow mesenchymal stromal cells promotes functional recovery and neuroplasticity after ischemic stroke in mice. *Sci Rep*. 2017;7:1-13.
50. Ghazavi H, Hoseini SJ, Ebrahimzadeh-Bideskan A, et al. Fibroblast growth factor type 1 (FGF1)-overexpressed adipose-derived mesenchaymal stem cells (AD-MSCFGF1) induce neuroprotection and functional recovery in a rat stroke model. *Stem Cell Rev Reports*. 2017;13:670-685.
51. Ishizaka S, Horie N, Satoh K, Fukuda Y, Nishida N, Nagata I. Intra-arterial cell transplantation provides timing-dependent cell distribution and functional recovery after stroke. *Stroke*. 2013;44:720-726.
52. Yang M, Wei X, Li J, Heine LA, Rosenwasser R, Iacovitti L. Changes in host blood factors and brain glia accompanying the functional recovery after systemic administration of bone marrow stem cells in ischemic stroke rats. *Cell Transplant*. 2010;19:1073-1084.
53. Liao W, Xie J, Zhong J, et al. Therapeutic effect of human umbilical cord multipotent mesenchymal stromal cells in a rat model of stroke. *Transplantation*. 2009;87:350-359.
54. Huang W, Mo X, Qin C, Zheng J, Liang Z, Zhang C. Transplantation of differentiated bone marrow stromal cells promotes motor functional recovery in rats with stroke. *Neurol Res*. 2013;35:320-328.
55. Hui ES, Du F, Huang S, Shen Q, Duong TQ. Spatiotemporal dynamics of diffusional kurtosis, mean diffusivity and perfusion changes in experimental stroke. *Brain Res*. 2012;1451:100-109.
56. Guglielmetti C, Veraart J, Roelant E, et al. Diffusion kurtosis imaging probes cortical alterations and white matter pathology following cuprizone induced demyelination and spontaneous remyelination. *Neuroimage*. 2016;125:363-377.
57. Zhuo J, Xu S, Hazelton J, et al. Diffusion kurtosis as an *in vivo* imaging marker for reactive astrogliosis in traumatic brain injury. *Neuroimage*. 2012;59:467-477.
58. Budde MD, Frank JA. Neurite beading is sufficient to decrease the apparent diffusion coefficient after ischemic stroke. *Proc Natl Acad Sci USA*. 2010;107:14472-14477.

SUPPORTING INFORMATION

Additional supporting information may be found online in the Supporting Information section.

FIGURE S1 Isotropic compartment from NODDI fit in the ipsilateral external capsule and striatum. Data displayed as means and SDs across all specimens in each group

FIGURE S2 Pearson's correlation coefficients for MD, AD, RD and FA in the external capsule. Coefficients were calculated by comparing DTI biometrics to the normalized distance traveled in the EPM

FIGURE S3 Pearson's correlation coefficients for ICVF and ODI in the external capsule and striatum. Coefficients were calculated by comparing NODDI biometrics to the normalized time spent within closed arms of the EPM

How to cite this article: Bagdasarian FA, Yuan X, Athey J, Bunnell BA, Grant SC. NODDI highlights recovery mechanisms in white and gray matter in ischemic stroke following human stem cell treatment. *Magn Reson Med*. 2021;00:1–13. https://doi.org/10.1002/mrm.28929